Influence of impurities on hydrodynamic solitons

Weizhong Chen,* Lei Lu, and Yifei Zhu
State Key Laboratory of Modern Acoustics and Institute of Acoustics, Nanjing University, Nanjing 210093, China
(Received 21 June 2004; revised manuscript received 29 October 2004; published 28 March 2005)

The interaction between impurities and solitary waves has been experimentally observed on the surface of a defective water layer subjected to vertical vibration. A slightly rugged surface on one sidewall of the water layer serves as the impurity, making the layer breadth at the defect slightly different elsewhere. A wide-breadth impurity will attract or pin not only the hydrodynamic breather at lower driving frequency, but also the kink at higher driving frequency, while a narrow-breadth one will repel them. Using a multiple scale expansion method, a nonlinear Schrödinger equation with an impurity term (NLSI) was derived from the basic hydrodynamic equation. Furthermore, we present numerical calculations that show good agreement between the NLSI-based theoretical model and the experimental results.

DOI: 10.1103/PhysRevE.71.036622 PACS number(s): 05.45.Yv, 47.20.Ky, 47.54.+r, 61.72.−y

I. INTRODUCTION

As is well known, homogeneous nonlinear systems support the undistorted localized waves, so-called solitons. These nonlinear systems include some continuous and discrete systems. Two typical samples, solitons in hydrodynamics [1,2] and the Frenkel-Kontorova (FK) model (the coupled pendulum chain) [3,4], have been widely studied in the past two decades. Theoretically, solitons have been well explained in the framework of the cubically nonlinear Schrödinger model (NLS) [3,5,6]. For the lattice, of course, it is necessary to use the long-wavelength limit or the continuum approximation to transform lattice equations to a differential equation. Since the 1990s, much attention has been paid to the FK chain with some impurities [7,8]. Up to now, some interesting impurity-soliton interactions (ISI) have been revealed by a number of theoretical and numerical investigations [3,9,10], based on the NLS with a δ impurity (NLSI) [9,10],

$$i\psi_t + \psi_{xx} + 2|\psi|^2\psi - \psi + 2q\delta(x)\psi - \gamma\psi^* + i\alpha\psi = 0, \quad (1)$$

where $|\psi|$ is the envelope amplitude, the subscripts stand for the partial differential with respect to them, α and γ are the damp coefficient and the driving strength, and q describes the relative strength of the impurity, respectively. Some impurity localized modes (ILM), nonlinear waves localized near the impurity, were also obtained analytically from Eq. (1) [7,8].

Our work is stimulated by the theoretical prediction of ISI [9,10] and ILM [7–9] from Eq. (1). Can we experimentally observe these ISI and ILM in a typical NLS-governed hydrodynamic system? In this paper, we are going to investigate the interactions between impurities and the hydrodynamic solitons including the breather [1] and kink [2].

II. INTERACTION BETWEEN SOLITONS AND IMPURITIES

The apparatus used in the present studies is similar to that described in more detail eslewhere [11,12]. A Plexiglas trough with the inner size of $765\times55\times80$ mm^3 is used to observe both breather and kink after being filled with water up to a depth of d. One sidewall of the trough is made up of double layers. The inner layer is made of two pieces of the Plexiglas boards with 4 mm thickness. Their size is about 379×80 mm^2. They are fixed on both ends of the outer layer. There is an interspace between two boards at the center of the trough. The width of the interspace $\Delta l=7$ mm is much smaller than the length of the trough $l=765$ mm. Then we insert a $7\times4\times80$ mm^3 Plexiglas bar into the gap between two boards, and the trough becomes a perfect one without any defect. The impurity here is an imhomogeneity in the breadth of the water layer, which is caused by the slight unevenness on one sidewall of the trough. In order to make a wide-breadth (convex) impurity of the water layer, we take out the inserted Plexiglas bar from the gap only. To form a narrow-breadth (concave) impurity of the water layer, we can put another Plexiglas bar on the inserted bar. Figure 1 shows the horizontal cross sections of water layers with impurities and their corresponding troughs. The thickness of the bars is adjustable and the typical thickness is 2–4 mm, which is also smaller than the breadth of the trough $b_0=55$ mm. The trough is then placed on a vertically vibrating plate. The vibrating apparatus is a typical Faraday resonance system [11,12].

For the water layer with specific breadth b_0 and depth d, the (0,1)-mode intrinsic frequency can be estimated by

$$\omega^2 = kg\tanh kd, \quad (2)$$

where wave number $k=\pi/b_0$, and g is the acceleration due to gravity. The intrinsic frequencies of the (0,1) mode, $f=\omega/2\pi$, are about 3.438 and 2,706 Hz for experimental layers with $b_0=55$ mm and $d=21$ mm and $d=10$ mm, respectively.

Before introducing an impurity, an appropriate frequency and amplitude were applied to the oscillating plate to excite a breather on the surface of the liquid layer in the trough, as observed usually [1] [see Fig. 2(a)]. In Fig. 2(a), we can see that the breather, whose center is at $x_0=-62$ mm, is smooth in profile. Then, we introduced a wide-breadth impurity at $x_i=0$ suddenly. The breather was then attracted from the pri-

*Electronic address: wzchen@nju.edu.cn

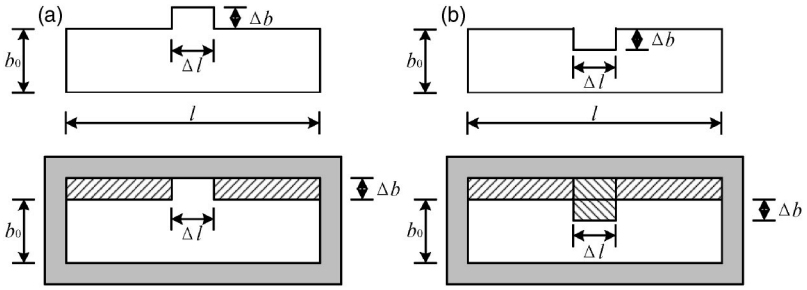

FIG. 1. The horizontal cross sections of the water layers with impurities (upper) and their corresponding troughs (lower). (a) A wide-breadth (convex) impurity; (b) a narrow-breadth (concave) one.

mary center x_0 to x_i. Meanwhile, the breather lost its smooth profile and became a distorted one [see Figs. 2(b) or 2(c)], that is, ILM [7]. The evolution duration from Figs. 2(a) (introducing the impurity) to 2(b) or 2(c) is relevant to the strength of the impurity, and its typical value is tens of seconds. However, if the breather was initially localized at the exact position where the wide-breadth impurity would be introduced (viz., $x_0=x_i$), it would remain stationary. The data in Fig. 3(a) record the evolution process that the wide-breadth impurities attract or pin the breathers. On the other hand, if we excited a perfect breather at $x_0=0$, and then introduced a narrow-breadth impurity at the same position (viz., $x_i=x_0=0$), the narrow-breadth impurity would repel the breather out of its center [see Fig. 3(b)]. The driving frequency $2f_e$ is about 6.550 Hz, which is slightly lower than the double intrinsic frequency of the perfect layer, say, $2f=6.876$ Hz.

Therefore, the experiments demonstrate that both wide- and narrow-breadth impurities are able to affect the breather. A wide-breadth impurity can attract or pin the breather, while the narrow one repels the breather at low frequency [lower than the double intrinsic frequency of the (0,1) mode].

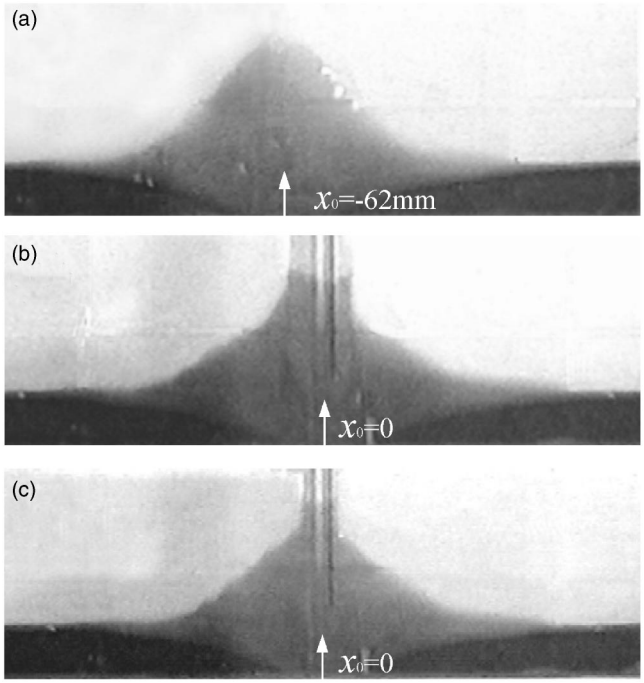

FIG. 2. The photos of the perfect and distorted breathers. (a) An initial perfect state; (b) a final state, the ILM described by $\mathrm{sech}(k|x|-\theta)$ with $\theta>0$ and k being a constant [7]; and (c) another final state, the ILM described by $\mathrm{sech}(k|x|-\theta)$ with $\theta<0$ [7].

Due to the topological difference, the interaction between the kink and impurities is inverse to that between the breather and impurities, in the numerical calculation based on the NLSI of a discrete system [10]. Then, the question is, what will happen in our experimental system?

In order to form a kink, we pumped some water out until $d=10$ mm, which means its (0,1)-mode intrinsic frequency is about 2.706 Hz. Increasing the driving amplitude A_e at $2f_e=5.427$ Hz, we observed a kink at $x_0=50$ mm; then a wide-breadth impurity ($\Delta b=5$ mm) was introduced at $x_i=0$. The wide-breadth impurity attracted the kink from x_0 to x_i (see Fig. 4). If the kink was originally located at $x_0=0$, the same position as the impurity ($x_i=0$), it would be pinned at $x_i=0$

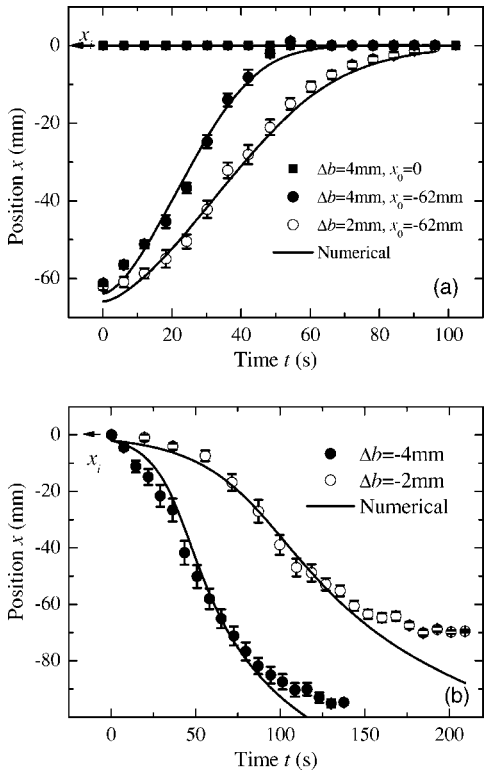

FIG. 3. The interactions between breather and impurities. (a) The breather is attracted or pinned by wide-breadth impurities ($\Delta b=4$ and 2 mm). (b) The breather is repelled by narrow-breadth impurities ($\Delta b=-4$ and -2 mm). The driving frequency $2f_e=6.550$ Hz, slightly lower than the double intrinsic frequency of the (0,1) mode for a perfect layer with $b_0=55$ mm and $d=21$ mm, and the driving amplitude $A_e=0.486$ mm. The curves show the numerical results with $N=131$.

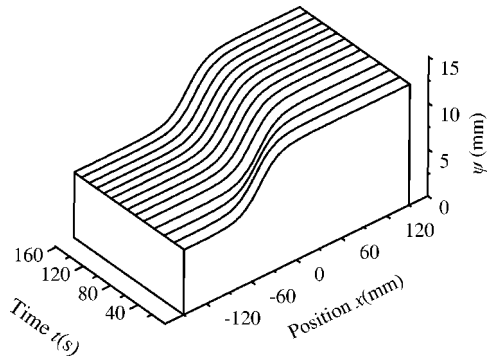

FIG. 4. The evolution of a kink near the wide-breadth impurity. The kink is initially at $x_0=-50$ mm, and is finally attracted to the position of the impurity, $x_i=0$, where $\Delta b=5$ mm, $2f_e=5.427$ Hz, and $A_e=1.596$ mm.

without any motion. Furthermore, we also observed that a kink would be repelled by a narrow-breather impurity ($\Delta b<0$ mm). The observation seems to suggest that the kink-impurity interaction is just the same as the breather-impurity interaction. It is a paradox that the interaction remains unchanged as the solitary wave changes from the breather to the kink, which is far away from the numerical prediction based on the FK chain [10]. In fact, the interaction rule in the hydrodynamic system here is completely consistent with the prediction from the FK chain, and can be explained using the resonant absorption picture [10]. We note that the half driving frequency $f_e=2.714$ Hz was higher than the intrinsic frequency of the kink ($f=2.706$ Hz) and rather lower than the intrinsic frequency of the breather. In other words, the wide-breadth impurity attracts the breather at low frequency, and it also attracts the kink at high frequency. As a straightforward deduction, the wide-breadth impurity should repel the kink at low frequency, which cannot be observed in the experiment, unfortunately [2].

The strength of the ISI, of course, is relevant to the strength of the impurities, say, the dimension of the defects Δb. There is a positive relation between them in our experimental region. Furthermore, the strength of the ISI also depends on the driving amplitude A_e. Figure 5 shows the strength (the displacement during 40 cycles) versus Δb and A_e.

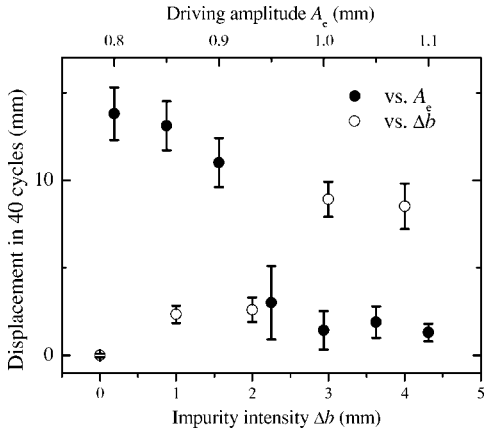

FIG. 5. The interaction strength on different impurity dimensions Δb and the driving amplitude A_e.

III. NONLINEAR SCHRÖDINGER EQUATION WITH BREADTH DEFECT

The theoretical model for the perfect hydrodynamic solitons was proposed by Larraza *et al.* [5] and Miles [6] since the hydrodynamic breather was discovered [1]. The perfect hydrodynamic soliton can be well explained in the framework of the forced and damped nonlinear Schrödinger equation [6], which is in the same form of Eq. (1) without the impurity term. For a liquid layer of uniform depth d and defective breadth $b(x)$ subjected to vertical vibration $A_e \cos 2\omega_e t$, we can write out the basic hydrodynamic equations,

$$\nabla^2\phi = 0 \text{ for } -d \leqslant z \leqslant \xi(x,y,z), \tag{3}$$

$$\phi_y = 0 \text{ at } y = 0, \tag{4}$$

$$\phi_y = 0 \text{ at } y = b(x), \tag{5}$$

$$\phi_z = 0 \text{ at } z = -d, \tag{6}$$

$$\xi_t - \phi_z + \phi_x\xi_x + \phi_y\xi_y = 0 \text{ at } z = \xi(x,y,t), \tag{7}$$

$$(g - 4A_e\omega_e^2\cos 2\omega_e t)\xi + \phi_t + \frac{1}{2}(\nabla\phi)^2 = 0 \text{ at } z = \xi(x,y,t), \tag{8}$$

where $\phi(x,y,z,t)$ and $\xi(x,y,t)$ are the velocity potential and the free surface displacement (relative to the trough) of the liquid layer, respectively. For a perfect liquid layer, $b(x)=b_0\equiv$ const. However, we are interested in the case of

$$b(x) = b_0[1 + \epsilon^2 f(x)] \equiv b_0 + F(x), \tag{9}$$

where the function $f(x)$ describes the shape of the defect, and ϵ is a small parameter. $f(x)>0$ stands for a positive (wide-breadth) impurity, and $f(x)<0$ for a negative (narrow-breadth) one.

As usual, we assume the wavy motion is small, $\phi(x,y,z,t)\sim\epsilon$, and $\xi(x,y,t)\sim\epsilon$, due to the driving amplitude $A_e=\epsilon^2 a_e\sim\epsilon^2$, is small. Furthermore, according to the experiments we set the half driving frequency ω_e very close to the intrinsic frequency of the dominant mode ω, that is, $(\omega_e^2-\omega^2)/2\omega=\epsilon^2\Delta\sim\epsilon^2$. Before taking up the multiple scales method, we should regularize the boundary curve of $y=b(x)$. We expand the boundary condition Eq. (5) at $y=b_0$, as done usually in the free surface conditions Eqs. (7) and (8). Then using the multiple scales method, we finally achieve an NLS with a breadth impurity $F(x)$ to describe the modulation amplitude along the x direction,

$$2i\omega\psi_t - \frac{g}{2k}[T + kd(1 - T^2)]\psi_{xx} - gk^2(1 - T^2)F(x)\psi + (\omega^2 - \omega_e^2)\psi + 2\alpha i\omega\psi - A|\psi|^2\psi - \frac{2\omega^4 A_e}{g}\psi^* = 0, \tag{10}$$

where

$$A = \frac{k^4}{8}(6T^4 - 5T^2 + 16 - 9T^{-2}), \tag{11}$$

with $T = \tanh kd$ (see the Appendix). In Eq. (10), α is introduced to describe the weak viscidity of fluid. The wavy motion can be written as

$$\xi(x,y,t) = \psi(x,t)\cos ky\ e^{i\omega t} + \text{c.c.}, \tag{12}$$

where c.c. denotes the complex conjugation. The coefficient of the cubic nonlinear term, A, determines the solitary waves to be a breather or a kink for a negative coefficient of the diffusive term. In other words, $\psi(x,t)$ gets a breather solution if $A > 0$, and a kink one if $A < 0$ [13]. Obviously, Eq. (10) has the same form as Eq. (1).

IV. NUMERICAL SIMULATION

Given the details of defect function $F(x)$, we can calculate the function $\psi(x,t)$ numerically. In the simulation, we used the implicit finite difference to represent approximately the partial differential with respect to spatial coordinate x; as a result, the partial differential equation (10) was transformed to a set of N ordinary differential equations (ODE) (N is the number of the mesh grid). Then we integrated the set of the ODEs by using the fifth-order Runge-Kutta algorithm as described in Ref. [14]. All experimentally measurable parameters were employed in the numerical computation except Δb. The phenomenological viscosity, α, was determined by fitting the experimental data, and was 0.46–0.48 s^{-1} in our calculation. The strength of the impurity served as adjustable parameters. The number of mesh N is related directly to the breadth of the impurity for a fixed number of the defective mesh. In our calculation, the number of the defective mesh was set to 2. The total number of the mesh was adjusted to fit the data.

In Fig. 3, we show the numerical results by curves. A good agreement with the experimental data has been achieved. Based on the numerical computation, it is easy to discuss the effect of the defect size $F(x)$ on the strength of the ISI. The result shows that the strength of the ISI weakens as the defect size decreases for a fixed breadth of the trough, which is quite understandable and consistent with the observation in Fig. 5.

Of course, we can also simplify the impurity function $F(x)$ by a Dirac $\delta(x)$ function and rescale the coordinates to arrive at Eq. (1), and extend the analytic method in Refs. [7,9] to study the ILM.

Furthermore, we note that the breadth impurity affects the hydrodynamic solitons by changing the intrinsic frequency in the impurity. So, we can also make some depth impurities to make changes in the intrinsic frequency, according to Eq. (2). A similar experiment has been performed to investigate the interaction between the depth impurity and solitons. The results show that a shallow impurity will attract breathers and kinks while a deep one will repel them, which is consistent with those of the breadth impurities (see Table I).

TABLE I. Effects of the breadth and depth impurities.

Solitons	Breadth impurity	Depth impurity	ISI
Breather $f_e < f$	Wide	Shallow	Attr.
	Narrow	Deep	Repel
Kink $f_e > f$	Wide	Shallow	Attr.
	Narrow	Deep	Repel

V. CONCLUSION AND DISCUSSION

In summary, we have investigated the interaction between the impurities and solitons on the surface of a defective layer of liquid subjected to parametric vibration. The experiments show that the wide-breadth impurity attracts the breather at lower driving frequency than the double intrinsic one. Similar interactions are observed in the case of the kink driven at higher frequency than the double intrinsic frequency. All of the regularity of ISI is completely consistent with that predicted numerically in the discrete FK model, which is understandable in the picture of the resonant absorption [10]. The ILM is also observed experimentally. In theory, from the hydrodynamic equation with a defective sidewall condition, a cubically nonlinear Schrödinger equation with an impurity $F(x)$ [a universal case including the Dirac $\delta(x)$ used usually] has been achieved by using perturbation technique. Due to the absence of the continuum approximation, Eq. (1) can describe the ISI in the hydrodynamic system better than that in the discrete lattice [12]. Therefore, all observations including ISI and ILM can be well reproduced in the framework of NLSI without exception. The experiment reported here strongly supports the theoretical conclusions in a serial of publications [8–10] on the ISI governed by NLSI.

ACKNOWLEDGMENTS

This work was supported in part by the National Nature Science Foundation of China (Grant No. 10374050) and the Special Funds for Major State Basic Research Project (973). The authors would like to thank Juan Tu of the University of Washington for her help in composition.

APPENDIX: DEDUCTION OF EQ. (10)

Although the basic hydrodynamic equations (3)–(8) are different from those in regular boundary conditions, they are also solved analytically by the perturbation technology. At first we introduce the slow variables x_1, x_2, t_1, t_2 as the following:

$$\frac{\partial}{\partial x} \to \epsilon \frac{\partial}{\partial x_1} + \epsilon^2 \frac{\partial}{\partial x_2} + \mathcal{O}(\epsilon^3) \tag{A1}$$

and

$$\frac{\partial}{\partial t} \to \frac{\partial}{\partial t_0} + \epsilon \frac{\partial}{\partial t_1} + \epsilon^2 \frac{\partial}{\partial t_2} + \mathcal{O}(\epsilon^3). \tag{A2}$$

At the same time, the functions ϕ and ξ are assumed to be small and can be expressed as

$$\phi(x,y,z,t) = \epsilon\phi_1(x_1,x_2,y,z,t_0,t_1,t_2) + \epsilon^2\phi_2(x_1,x_2,y,z,t_0,t_1,t_2) + \epsilon^3\phi_3(x_1,x_2,y,z,t_0,t_1,t_2) + \mathcal{O}(\epsilon^4) \tag{A3}$$

and

$$\xi(x,y,t) = \epsilon\xi_1(x_1,x_2,y,t_0,t_1,t_2) + \epsilon^2\xi_2(x_1,x_2,y,t_0,t_1,t_2) + \epsilon^3\xi_3(x_1,x_2,y,t_0,t_1,t_2) + \mathcal{O}(\epsilon^4). \tag{A4}$$

Before expanding them, we homogenize the boundary conditions on the defective sidewall and the free surface as well. Equations (5), (7), and (8) are expanded into Taylor serials at their corresponding regular planes, that is,

$$\phi_y - \epsilon^2[b_0F_x\phi_x + \phi_{yy}b_0F] + \mathcal{O}(\epsilon^4) = 0 \text{ at } y = b_0, \tag{A5}$$

$$\xi_t - \phi_z + \phi_x\xi_x + \phi_y\xi_y - \phi_{zz}\xi + \phi_{xz}\xi\xi_x + \phi_{yz}\xi\xi_y - \frac{1}{2}\phi zzz\xi^2 + \mathcal{O}(\epsilon^4) = 0 \text{ at } z = 0, \tag{A6}$$

and

$$\phi_t + g(1 + 4\omega_e^2 a_e \epsilon^2 \cos 2\omega_e t)\xi + \frac{1}{2}\left[(\phi_x)^2 + (\phi_y)^2 + (\phi_z)^2\right] + \phi_{zt}\xi + [\phi_x\phi_{xz} + \phi_y\phi_{yz} + \phi_z\phi_{zz}]\xi + \frac{1}{2}\phi_{zzt}\xi^2 + \mathcal{O}(\epsilon^4) = 0, \quad \text{at } z = 0. \tag{A7}$$

Substituting Eqs. (A1)–(A4) into Eqs. (3), (4), (6), and (A5)–(A7), we obtain a chain of equations in different orders of ϵ. The equations in the first order are the following:

$$\phi_{1yy} + \phi_{1zz} = 0 \text{ for } (-d \leqslant z \leqslant 0), \tag{A8}$$

$$\phi_{1y} = 0 \text{ at } y = 0, \tag{A9}$$

$$\phi_{1y} = 0 \text{ at } y = b_0, \tag{A10}$$

$$\phi_{1z} = 0 \text{ at } z = -d, \tag{A11}$$

$$\xi_{1t_0} - \phi_{1z} = 0 \text{ at } z = 0, \tag{A12}$$

$$\phi_{1t_0} + g\xi_1 = 0 \text{ at } z = 0, \tag{A13}$$

so the solutions are

$$\phi_1 = \psi \cos ky \frac{\cosh k(z+d)}{\cosh kd} e^{i\omega t_0} + \text{c.c.} \tag{A14}$$

and

$$\xi_1 = -i\frac{\omega}{g}\psi \cos ky\ e^{i\omega t_0} + \text{c.c.}, \tag{A15}$$

where c.c. stands for the complex conjugate, and $\psi = \psi(x_1, x_2, t_1, t_2)$ is a function of slow variables. In order to determine the ψ, we will go on solving the equations in the higher orders of ϵ.

The equations in the order of ϵ^2 are

$$\phi_{2yy} + \phi_{2zz} = 0 \text{ for } (-d \leqslant z \leqslant 0), \tag{A16}$$

$$\phi_{2y} = 0 \text{ at } y = 0, \tag{A17}$$

$$\phi_{2y} = 0 \text{ at } y = b_0, \tag{A18}$$

$$\phi_{2z} = 0 \text{ at } z = -d, \tag{A19}$$

$$\xi_{2t_0} - \phi_{2z} = \phi_{1zz}\xi_1 - \phi_{1y}\xi_{1y} - \xi_{1t_1} \text{ at } z = 0, \tag{A20}$$

$$\phi_{2t_0} + g\xi_2 = -\phi_{1t_1} - \frac{1}{2}\left[\phi_{1y}^2 + \phi_{1z}^2\right] - \phi_{1t_0z}\xi_1 \text{ at } z = 0. \tag{A21}$$

The solutions to Eqs. (A16)–(A21) can be easily written as

$$\phi_2 = \frac{ik^2}{8\omega}\left[3\left(T^2 - T^{-2}\right)\cos 2ky \frac{\cosh 2k(z+d)}{\cosh 2kd} + \left(1 + 3T^2\right)\right]\psi^2 e^{2i\omega t_0} + \text{c.c.} \tag{A22}$$

and

$$\xi_2 = \left[\frac{k^2\psi^2}{4g}\left(1 - 3T^{-2}\right)\cos 2ky\ e^{2i\omega t_0} + \text{c.c.}\right] + \frac{k^2|\psi|^2}{2g}\left[\left(1 + T^2\right)\cos 2ky - \left(1 - T^2\right)\right], \tag{A23}$$

with $T = \tanh kd$.

The equations in the order of ϵ^3 are

$$\phi_{3yy} + \phi_{3zz} = -\phi_{1x_1x_1} \text{ for } (-d \leqslant z \leqslant 0), \tag{A24}$$

$$\phi_{3y} = 0 \text{ at } y = 0, \tag{A25}$$

$$\phi_{3y} = -\phi_{1yy}b_0 f(x_1,x_2) \text{ at } y = b_0, \tag{A26}$$

$$\phi_{3z} = 0 \text{ at } z = -d, \tag{A27}$$

$$\xi_{3t_0} - \phi_{3z} = f_1 \text{ at } z = 0, \tag{A28}$$

$$\phi_{3t_0} + g\xi_3 = f_2 \text{ at } z = 0, \tag{A29}$$

where the known functions f_1 and f_2 are defined as

$$f_1 \equiv -\xi_{2t_1} + \phi_{1zz}\xi_2 + \phi_{2zz}\xi_1 + \frac{1}{2}\phi_{1zzz}\xi_1^2 - \phi_{1y}\xi_{2y} - \phi_{2y}\xi_{1y} - \phi_{1yz}\xi_1\xi_{1y} - \xi_{1t_2} \tag{A30}$$

and

$$f_2 \equiv -4g\omega_e^2 a_e \cos 2\omega_e t_0 \xi_1 - \phi_{2t_1} - \phi_{1t_2} - \phi_{1zt_0}\xi_2 + [(\phi_{2zt_0} + \phi_{1zt_1})]\xi_1 - [(\phi_{1z}\phi_{1zz} + \phi_{1y}\phi_{1yz})]\xi_1 - \phi_{1z}\phi_{2z} - \frac{1}{2}\phi_{1zzt_0}\xi_1^2 - \phi_{1y}\phi_{2y}. \quad \text{(A31)}$$

The surface function ξ_3 can be eliminated through Eqs. (A28) and (A29), and the boundary condition of ϕ_3 on the surface $z=0$ becomes

$$\phi_{3t_0t_0} + g\phi_{3z} = f_{2t_0} - gf_1. \quad \text{(A32)}$$

Although the third-order equations (A24)–(A27) and (A32) with Eqs. (A30) and (A31) are quite complicated, especially the asymmetrical conditions between two sidewalls at $y=0$ and $y=b_0$, fortunately we have found an explicit expression of the fundamental motion of ϕ_3 as the following:

$$\phi_3 = \left[(z+d)\psi_{x_1x_1}\cos ky \frac{\sinh k(z+d)}{2k\cosh kd} + ky\psi \sin ky \frac{\cosh k(z+d)}{\cosh kd} f(x_1,x_2) - k(z+d)\psi \cos ky \frac{\sinh k(z+d)}{\cosh kd} f(x_1,x_2) \right] e^{i\omega t_0} + \text{c.c.} \quad \text{(A33)}$$

The balance in the fundamental motion of Eq. (A32) gives out a limitative equation for the function ψ,

$$2i\omega\epsilon^2\psi_{t_2} - \frac{g}{2k}\left[T + kd\left(1-T^2\right)\right]\epsilon^2\psi_{x_1x_1} - gk^2\left(1-T^2\right)\epsilon^2 f(x)\psi + \epsilon^2\Delta\psi + 2i\omega\alpha'\epsilon^2\psi - A|\psi|^2\psi - \frac{2\omega^4}{g}\epsilon^2 a_e\psi^* = 0. \quad \text{(A34)}$$

Substituting $\epsilon^2 t = t_2$, $\epsilon x = x_1$ and $\epsilon^2 a_e = A_e$, $\epsilon^2\Delta = (\omega^2 - \omega_e^2)/2\omega$, $\epsilon^2\alpha' = \alpha$, we recover the slow variables into their original ones, and transfer Eq. (A34) into Eq. (10).

[1] J. R. Wu, R. Keolian, and I. Rudnick, Phys. Rev. Lett. **52**, 1421 (1984).
[2] B. Denardo, W. Wright, S. Putterman, and A. Larraza, Phys. Rev. Lett. **64** 1518 (1990).
[3] O. M. Braun and Y. S. Kivshar, Phys. Rep. **306**, 1 (1998).
[4] D. Hennig and G. P. Tsironis, Phys. Rep. **307**, 333 (1999).
[5] A. Larraza and S. Putterman, J. Fluid Mech. **148**, 443(1984).
[6] J. W. Miles, J. Fluid Mech. **148**, 451 (1984).
[7] O. Braun and Y. S. Kivshar, Phys. Rev. B **43**, 1060 (1991).
[8] R. Scharf and A. R. Bishop, Phys. Rev. A **43**, 6535 (1991).
[9] N. V. Alexeeva, I. V. Barashenkov, and G. P. Tsironis, Phys. Rev. Lett. **84**, 3053 (2000).
[10] W. Z. Chen, B. B. Hu, and H. Zhang, Phys. Rev. B **65**, 134302 (2002).
[11] W. Z. Chen, R. J. Wei, and B. R. Wang, Phys. Rev. E **53**, 6016 (1996).
[12] W. Z. Chen, Y. F. Zhu, and L. Lu, Phys. Rev. B **67**, 184301 (2003).
[13] M. Remoissenet, *Waves Called Solitons*, 2nd ed. (Springer-Verlag, Berlin, 1996).
[14] W. H. Press, S. A. Teukolsky, W. T. Vetterling, and B. P. Flannery, *Numerical Recipes in C*, 2nd ed. (Cambridge University Press, Cambridge, 1997).